Relationship between the Electrochemical Behavior and Li Arrangement in $Li_xM_yMn_{2-y}O_4$ (M = Co, Cr) with Spinel Structure

Tomoaki Kashiwagi,[†] Masanobu Nakayama,[†] Kyohei Watanabe,[†] Masataka Wakihara,*[,†] Yo Kobayashi,[‡] and Hajime Miyashiro[‡]

Department of Applied Chemistry, Tokyo Institute of Technology, Ookayama, Meguro-ku, Tokyo 152-8552, Japan, and Materials Science Research Laboratory, Central Research Institute of Electric Power Industry, 2-11-1, Iwado Kita, Komae-shi, Tokyo 201-8511, Japan

Received: November 2, 2005; In Final Form: January 16, 2006

The relationship between the electrochemical behavior and the arrangement of lithium/vacancies has been investigated with electrochemical Li removal in $Li_xM_yMn_{2-y}O_4$ ($x \leq 1.0$, $0.0 \leq y \leq 0.3$, M = Co, Cr). It was shown that the electrochemical removal proceeds via two voltage regions: (1) ~3.9 V at $x \geq \sim 0.5$ and (2) ~4.2 V at $x \leq \sim 0.5$. To understand the stepwise behavior, entropy measurement of reaction, ΔS_{obs}, was performed by using the electrochemical methods. The changes of the sign in ΔS_{obs} from negative to positive at the composition $x \sim 0.50$ in $Li_xM_yMn_{2-y}O_4$ indicated that the ordered arrangement of Li/vacancies was formed with electrochemical Li removal. Moreover, such an ordering was suppressed by the substitution of Co^{3+} and Cr^{3+} for Mn^{3+}. To clarify the nature and origin of Li/vacancy ordering, the Monte Carlo simulation was performed in view of Coulombic interaction. The simulation reproduced the formation of a new phase arising from Li/vacancy ordering at $x = 0.50$ in $Li_xMn_2O_4$. In addition, the ordered arrangement of Li/vacancy at $x = 0.5$ was perturbed by the trivalent M^{3+} replacement in spinel structure due to the local clustering of Li^+ around M^{3+}. Consequently, the electrochemical behavior in spinel $LiMn_2O_4$ was deeply related to the Coulombic interactions, proved by the fact that experimentally observed changes in entropy agreed well with Monte Carlo simulation based on the Coulombic interaction.

Introduction

Development of the cathode materials for Li ion battery is vital to meet the demands of portable devices, future usages of electric vehicles, and so on. Among the cathodes, $LiMn_2O_4$ and related oxides have gained much attention because of their low cost, low toxicity, and relatively high energy density.[1−6] The structure of $LiMn_2O_4$ belongs to the spinel type structure (space group $Fd\bar{3}m$) in which oxygen forms cubic closed packing (ccp) and Mn and Li distributed in half of octahedral site (16d site) and $^1/_8$ of tetrahedral site (8a site), respectively (see, Figure 1). During electrochemical charging and discharging, this material undergoes reversible lithium removal/insertion without changing the flame structure of Mn_2O_4.[7] Although no significant structural changes were observed in this electrochemical reaction, measured potentials as a function of lithium content showed sudden increase from ~3.9 to ~4.2 V at $x \sim 0.5$.[7] Gao et al. reported that this phenomenon stemmed from the ordered arrangement of Li/vacancies with the results of electrochemical behavior and Monte Carlo simulation with empirical parameters of the lattice gas model.[8] In this respect, the measurement of configurational entropy of reaction is one of the effective ways to investigate the ordering nature of $Li_xMn_2O_4$ quantitatively. Newman's group has measured the entropy of reaction and performed the Monte Carlo simulation using Dahn's model, showing good accordance between experimental and computational results.[9,10] However, a question still exists, what kind of interaction leads to the formation of ordered structure, because their Monte Carlo simulation only takes into account the first and second neighbor interactions, and the potential parameters they used were estimated empirically. In addition, Van der Ven et al.[11] and Ammundsen et al.[12] supported this idea by using ab initio theoretical computation and spectroscopic methods, respectively, whereas Neutron diffraction patterns for half-delithiated samples showed no diffraction peak arising from superstructure formation of Li ordering reported by Liu et al.[13] and Berg et al.[14] Thus, the formation of ordered arrangement of Li/vacancies is still controversial.

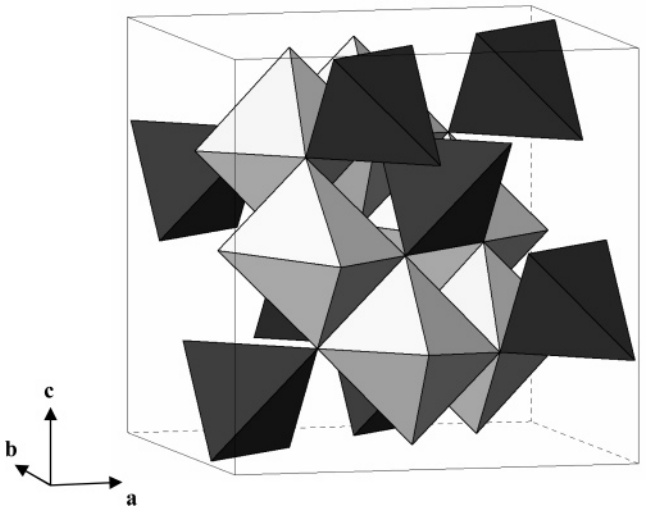

Figure 1. Crystal structure of spinel $LiMn_2O_4$. Brighter octahedron and darker tetrahedron indicate MnO_6 and LiO_4 units, respectively.

* Address correspondence to this author.
[†] Tokyo Institute of Technology.
[‡] Central Research Institute of Electric Power Industry.

10.1021/jp056334y CCC: $33.50
Published on Web 02/11/2006

Another aspect of interest around $LiMn_2O_4$ materials is a metal substitution effect that improves the cycle performance for the usage of the lithium ion battery.[15] The exact reasons for the improvements are still ambiguous, but Gummow et al.[6] and Li et al.[15] have pointed out the enhancement of the phase stability leads to good cyclability. Thus, the basic study regarding thermodynamics of $LiMn_2O_4$ and its relatives is important to understand their electrochemical behavior.

In the present study, we examined entropy measurement of reaction for the spinels, $LiMn_2O_4$, and trivalent metal doped ones, $LiCo_yMn_{2-y}O_4$ and $LiCr_yMn_{2-y}O_4$. In addition, to discuss the origin of ordered arrangement of Li/vacancies, Monte Carlo simulation was performed based on the Coulombic interaction.

Experimental Section

The samples of $LiM_yMn_{2-y}O_4$ ($y = 0$, 0.05, 0.15, 0.30; M = Co, Cr) were prepared by conventional solid-state reaction, and details have already been reported in the references.[16,17] The mixture of stoichiometric amounts of Li_2CO_3, Co_2O_3, Cr_2O_3, and Mn_2O_3 (which was prepared by preheating of $MnCO_3$ at 600 °C for 24 h) was used as the starting material. The mixture was heated at 820 °C for 3 days in air, then cooled at a rate of 0.5 deg/min. The phase identification and evaluation of lattice parameters were carried out by powder X-ray diffraction (XRD) technique, using Cu Kα radiation (RINT-2500V, Rigaku Co. Ltd).

The open circuit potential (OCP) data were measured with a three-electrode type cell. The working electrode was a mixture of 70 wt % sample powder, 25 wt % acetylene black (AB) as a current collector, and 5 wt % poly(tetrafluoroethylene) (PTFE) as a binder, and the total weight of the materials was ∼100 mg to obtain the accurate molar amount of electrochemically removed lithium ions. Li foil (Aldrich) was used for the counter and the reference electrodes, and 1 M $LiClO_4$ in ethylene carbonate (EC) and diethylene carbonate (DEC) was used as the electrolyte solution (Tomiyama Pure Chemical Company, Limited). The cell was charged with the current density of 0.05 C, and then the potential was relaxed for 6 h. The measured potential after relaxation was used as the OCP, E_{OCP}, for the corresponding composition x.

The entropy of reaction was estimated by the measurement of temperature dependence on OCP. The relationship between the OCP, E_{OCP}, and changes in the entropy of reaction, ΔS, is given by following equation

$$\left(\frac{\partial E_{OCP}}{\partial T}\right)_P = \frac{\Delta S}{nF} \quad (1)$$

where T, n, and F indicate temperature, number of electrons participating in the reaction (in this case, $n = 1$), and Faraday constants. In the present study, the measurement of the entropy was performed along with the electrochemical method referring to the method of Thomas et al.[9] A coin-type cell was used because of its good heat conduction. For the working electrode, spinel powder, AB, and polyvinylidenfluoride (PvdF) binder were mixed at a weight ratio of 8:1:1 and dissolved into *N*-methylpyrrolidone (NMP). The slurry was coated onto a pure aluminum sheet dried at 120 °C in air for 12 h to vaporize the NMP, then cut into a disk. This disk with ∼10 mg of active material was used as the working electrode. Lithium metal and 1 M $LiClO_4$ in EC/DEC were used as a counter electrode and electrolyte solution, respectively. The entropy measurement of reaction was performed according to the following temperature cycling operation. The cell was initially charged at a constant current of 0.05 C up to the various composition x in $Li_xM_yMn_{2-y}O_4$ at 298 K in a thermostat. Next, the potential was relaxed for 6 h at the same temperature. To avoid the error of estimation of composition x, the molar amount of Li was again evaluated by using the OCP data obtained by a three-electrode cell. (Note that quite small amounts of sample were used in coin-type cells for the entropy measurement of reaction. Therefore, it leads to a large error for the evaluation of composition x, due to the self-discharge reaction and so on.) After 6 h of relaxation, the temperature was linearly varied at a rate of 5 deg/h with the following three steps: the temperature was (1) raised from 298 to 303 K, (2) decreased from 303 to 293 K, and (3) raised again from 293 to 298 K. The results of the temperature dependence of the potential were fitted by the linear function, and the entropy of reaction ΔS_{obs} was obtained from eq 1. Note that gradual potential decrease (ca. −0.001 V/h) takes place during the relaxation step because of self-discharging.[8] To correct for the continual decrease of the cell potential, the potential profile of 298 K before and after temperature cycling was extrapolated by quadratic functions. The obtained potential profile during temperature cycling was subtracted from the approximated quadratic functions, and this corrected potential was used for the evaluation of ΔS_{obs}.

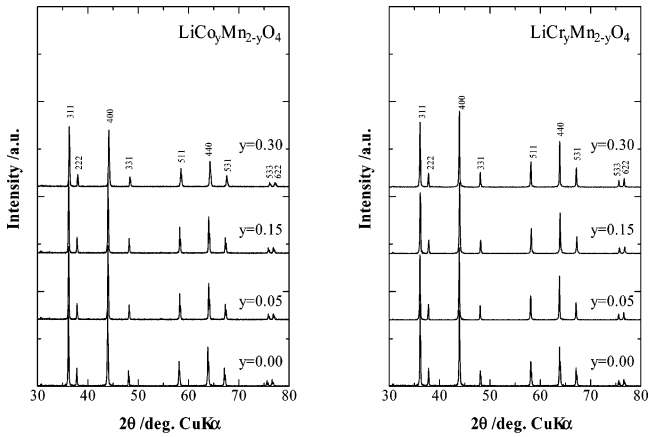

Figure 2. Powder X-ray diffraction patterns for $LiCo_yMn_{2-y}O_4$ and $LiCr_yMn_{2-y}O_4$ ($0 \le y \le 0.3$).

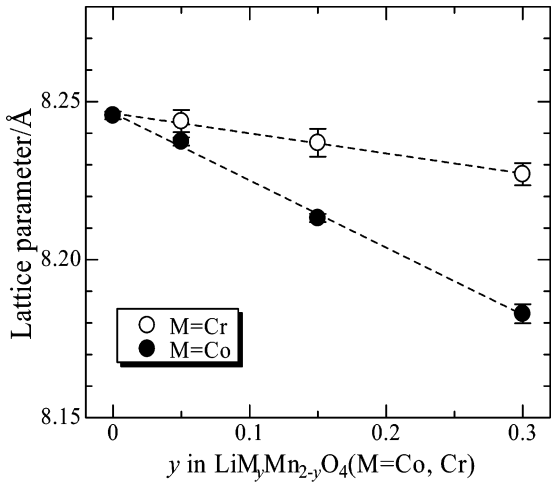

Figure 3. Variation of the lattice parameter as a function of y in $LiM_yMn_{2-y}O_4$ (M = Co, Cr).

Results

The results of powder XRD for $LiM_yMn_{2-y}O_4$ (M = Co, Cr; $y = 0$, 0.05, 0.15, 0.30) are shown in Figure 2. The XRD patterns

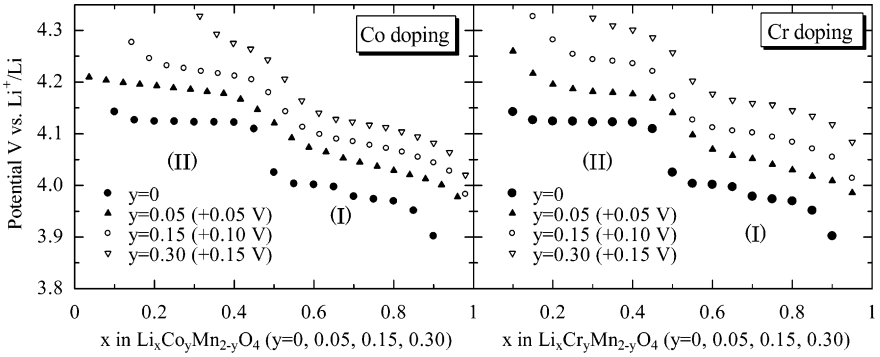

Figure 4. Variation of the equilibrium potential for $Li_xM_yMn_{2-y}O_4$ (M = Co, Cr). For the sake of comparison, to the potentials of the samples with the composition $y = 0.05$, 0.15, and 0.30 were added the values +0.05, +0.10, and +0.15 V, respectively.

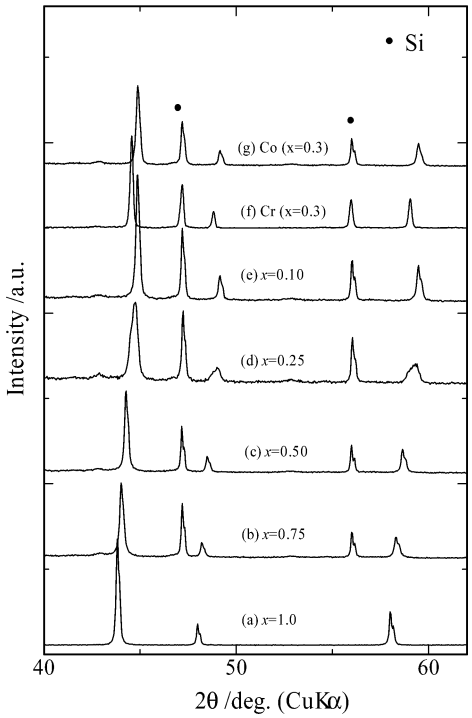

Figure 5. Ex situ XRD for (a−e) $Li_xMn_2O_4$, (f) $Li_{0.3}Cr_{0.3}Mn_2O_4$, and (g) $Li_{0.3}Co_{0.3}Mn_2O_4$. Si powder was used as an internal standard.

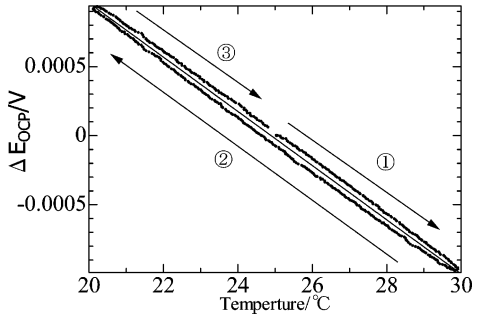

Figure 6. Typical example of the variation of the OCP at the compsition $x = 0.8$ in $Li_xMn_2O_4$ during temperature cycling.

of $LiMn_2O_4$ showed a good accordance with reported results of spinel $LiMn_2O_4$.[18,19] The peaks are gradually shifted to the higher angle region, and no split of the peaks was observed with doping with Co and Cr ions. Thus, it was confirmed that only the single spinel phase was obtained in this compositional range ($0 \le y \le 0.3$). The variation of refined lattice parameter was presented in Figure 3. The observed lattice parameters were linearly decreased with doping, and the lattice parameters of Co-doped spinels were smaller than those of Cr-doped ones.

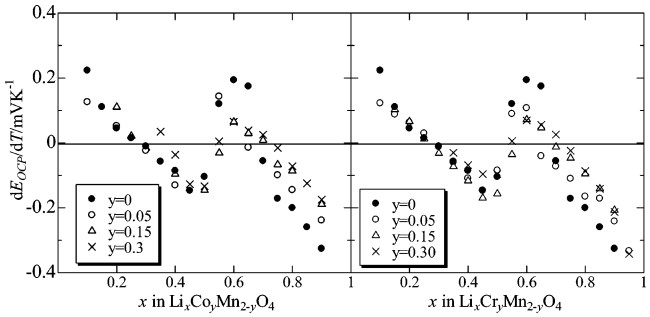

Figure 7. dE_{OCP}/dT as a function of x in $Li_xM_yMn_{2-y}O_4$ (M = Co, Cr). The composition x was evaluated by referring to the OCP after 6 h relaxiation measured by a three-electrode cell as mentioned in the Experimental Section. Only the x values at the range of $\sim 0.1 \le x \le \sim 0.5$ for $Li_xMn_2O_4$ were evaluated from the integrated charging current with use of Faraday's law, since no changes in OCP were observed (two-phase coexistence reaction).

Such behavior can be understood by the idea of ionic radii. Since the radii of trivalent Co^{3+}, Cr^{3+}, and Mn^{3+} ions are 0.685, 0.755, and 0.785, respectively,[20] the replacement of Mn^{3+} by Co^{3+} and Cr^{3+} causes the shrinkage of the cell, and Cr^{3+} doping leads to a smaller decrease in the lattice parameter than Co^{3+} doping does.

The OCP of the samples, $Li_xM_yMn_{2-y}O_4$, are presented in Figure 4. Two potential regions of electrochemical reactions are distinctly observed in the OCP diagrams of $Li_xMn_2O_4$, showing ca. 3.9 V at the composition $x > \sim 0.5$ (region I) and ca. 4.1 V at $x < \sim 0.5$ (region II), respectively. The OCP of region I in $Li_xMn_2O_4$ showed a gradual increase with composition x, indicating the solid solution reaction proceeded. On the other hand, the OCP of region II remained constant during the composional range of $\sim 0.1 < x < \sim 0.5$. Therefore, a two-phase reaction, $Li_{\sim 0.5}Mn_2O_4 \rightarrow Li_{\sim 0.1}Mn_2O_4 + \sim 0.4Li$, was indicated in region II of $Li_xMn_2O_4$. This electrochemical behavior is consistent with the previous report by Ohzuku et al.[7] No significant change was observed in the averaged potential for each two-potential region in Co- or Cr-doped samples. However, by doping of Co or Cr ions into Mn sites, the features of the two-potential region were fading a little, or the potential monotonically increases with Li removal compared with that of $Li_xMn_2O_4$. Additionally, the two-phase coexistence reaction mechanism in region II of $Li_xMn_2O_4$ changed to a solid−solution type reaction in Co- or Cr-doped spinels. (Note that the molar amount of lithium ions removed with the charging decreased with substitution in the present cutoff voltage region, since the molar number of Mn^{3+} ions in $LiM_yMn_{2-y}O_4$ which contribute to oxidation/reduction with Li removal/insertion decreased with substitution of trivalent Co^{3+} or Cr^{3+} ions. On the other hand,

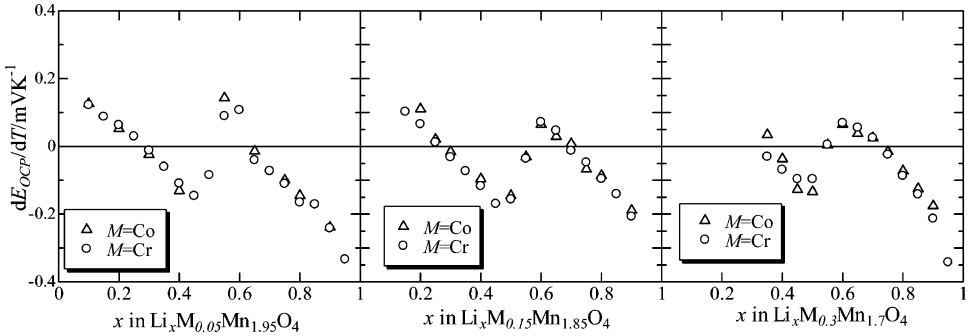

Figure 8. dE_{OCP}/dT as a function of x for Co or Cr doped spinels. Good accordance was observed in the values of dE_{OCP}/dT when the amount of Co and Cr doping is equal.

only Mn^{3+} ions in $LiM_yMn_{2-y}O_4$ varied their oxidation state from 3+ to 4+ in this voltage region.)

The structural change with lithium insertion was evaluated by ex situ XRD, and the results are shown in Figure 5. Since the peak feature of the patterns was roughly unchanged with Li removal, the host structure of $Li_xM_yMn_{2-y}O_4$ keeps its framework upon Li removal. In detail, the broad peaks were observed in $Li_xMn_2O_4$ between $x = \sim 0.1$ and ~ 0.4, indicating split of the peaks arising from the two-phase coexistence. On the other hand, no peak split was observed in the corresponding composition x in Co- or Cr-doped samples. Therefore, it was confirmed that the two-phase coexistence reaction took place in region II of $Li_xMn_2O_4$, whereas the solid solution type reaction proceeded at the corresponding composition ($x < \sim 0.5$) of Co- or Cr-doped samples as indicated by the OCP measurement mentioned above (Figure 3).

Figure 6 shows an typical example of the potential change during temperature cycling, and the variation can be approximated by a linear function. Although the small hysteresis could be due to the delay of heat response observed, the effect of this hysteresis would be canceled by averaging the potential data of both the temperature increasing and decreasing cycles. In addition, no marked change was observed in the plot of Figure 6, when the rate of temperature cycling was slowed to 5 deg/min, so that the relaxation for the change of temperature is fast enough to obtain the equilibrium state. The gradient with various composition x (dE_{OCP}/dT, Figure 6) is proportional to the entropy of reaction, ΔS_{obs}, along with eq 1. (Note that this ΔS_{obs} includes the contribution of the reaction at the counter electrode. However, this contribution to ΔS_{obs} is considered to be constant in the whole compositional region, because the same metal solvation/deposition reaction, $Li \rightarrow Li^+ + e^-$, proceeds at the counter electrodes.)

The obtained dE_{OCP}/dT of $Li_xMn_2O_4$ was plotted as a function of composition x in Figure 7. The measured dE_{OCP}/dT is initially negative around $x \sim 1.0$ and increased with lithium removal to be positive around $x \sim 0.7$. Then a sudden decrease in dE_{OCP}/dT was recognized at $x \sim 0.5$ where the change in OCP was observed, leading to a negative value of dE_{OCP}/dT. In region II where the two-phase coexistence reaction took place, the dE_{OCP}/dT monotonically increased with Li removal. (Note that the interpretation for the variation of dE_{OCP}/dT in the two-phase coexistence region is unclear. Maybe it contains the boundary formation of the two-phase domain in the crystal and so on.) The observed behavior of dE_{OCP}/dT for parent $LiMn_2O_4$ showed good agreement with previous results.[9] Therefore the two potential features observed in the OCP diagram would stem from the remarkable change in the ΔS_{obs} at $x \sim 0.5$ because of one-to-one correspondence in potential change at $x \sim 0.5$.

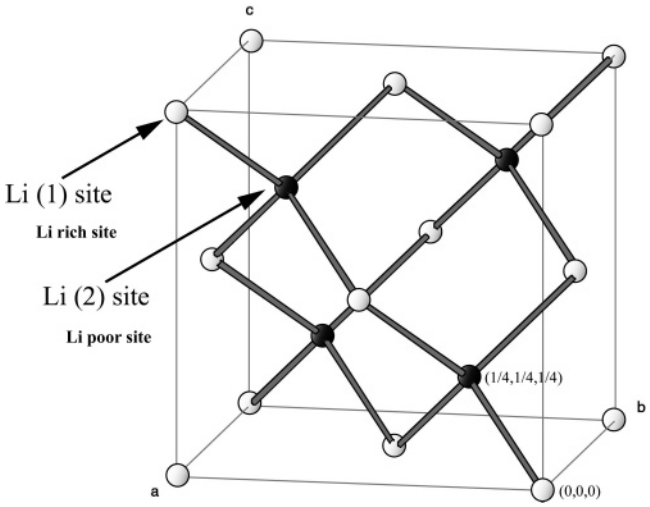

Figure 9. Schematic figure of the Li/vacancy ordering arrangement in the 8a site of the spinel structure ($Fd3m$). The Li(1) sites were occupied by a larger number of Li ions than the Li(2) sites.

For the samples of Co and Cr doping, the measured dE_{OCP}/dT was also shown in Figure 7, indicating similar behavior qualitatively to that of $Li_xMn_2O_4$. However, the changes in the absolute value of dE_{OCP}/dT became smaller with an increase in Co or Cr doping in the spinel. For example, the local maximum value of dE_{OCP}/dT around $x \sim 0.6$ decreased with Co and Cr doping (Figure 7). In addition, the value of dE_{OCP}/dT agreed with that of Co- and Cr-doped samples when the same amount of trivalent cation M^{3+} (Co^{3+} or Cr^{3+}) was doped in the spinel, even though the lattice parameter is different for each. (To confirm this, we replotted the dE_{OCP}/dT of $Li_xM_yMn_{2-y}O_4$ with the same y of Co and Cr doping as shown in Figure 8.)

Discussion

Hereafter, we discuss the details of the change in entropy of the reaction. Two conceivable effects contribute to the changes in entropy of the reaction: (1) vibrational and (2) configurational effects. Since the behavior of the entropy of reaction with x does not depend on the lattice parameter of spinels but on the molar amount of substitution y for both trivalent cations, M (see Figures 7 and 8), the contribution of vibrational entropy is negligibly small in this case. On the other hand, the configurational effect arising from the distribution of Li and vacancies is not directly related to the lattice parameter and that of doping metals. In this respect, it was suggested that the superstructure due to Li/vacancy ordering formed at the composition $x = 0.5$ in $Li_xMn_2O_4$, where Li ions alternatingly occupy the tetrahedral 8a sites (see Figure 9) as proposed previously.[7] Considering the extreme condition of this model, the entropy of the reaction

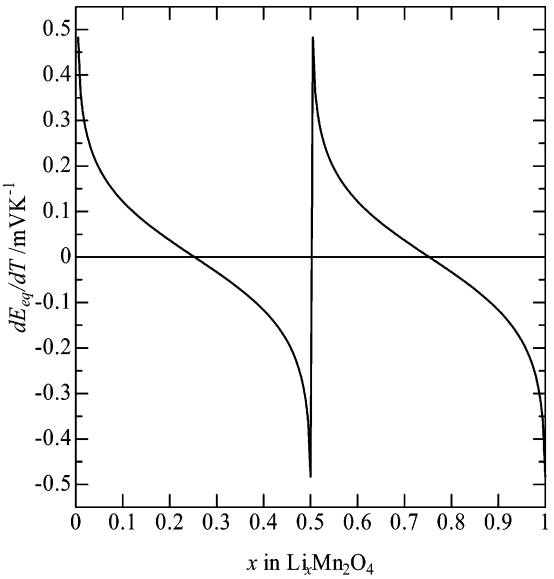

Figure 10. Simulated dE_{OCV}/dT as a function of composition x in $Li_xMn_2O_4$, when Li ions selectively remove from initially Li-(2) sites and then the Li(1) site (see Figure 9).

TABLE 1: Structural Parameters and Charge Distribution in $Li_xM_yMn_{2-y}O_4$ for the Monte Carlo (MC) Simulation and Coulombic Energy Calculation, Using Averaged Charge (AVC) Distribution

site	ion	occupancy	charge for MC	charge for AVC	fractional coordinates
8a	Li	x	+1	x	0, 0, 0
8a	vacancy	$1-x$	0	x	0, 0, 0
16d	M	$y/2$	+3	$3.5-x/2$	5/8, 5/8, 5/8
16d	Mn	$1-(y/2)$	$(7-x-3y)/(2-y)$	$3.5-x/2$	5/8, 5/8, 5/8
32e	O	1	−2	−2	3/8, 3/8, 3/8

would vary as presented in Figure 10. The simulated dE_{OCP}/dT was qualitatively similar to the observed dE_{OCP}/dT, so that the variation of the entropy of reaction would be explained by the order/disorder arrangement of Li and vacancy in the tetrahedral 8a site network of spinel $Li_xMn_2O_4$.

As mentioned in the previous section, the shape of the measured dE_{OCP}/dT was unchanged but the value increased as y increased in $Li_xM_yMn_{2-y}O_4$. Hence the degree of the ordering/disordering of Li/vacancy would be affected by the changes in host structure as indicated in the previous results. In detail, the variation of the measured dE_{OCP}/dT depended only on composition y and not the sort of metal (Co or Cr) or lattice parameter. The common feature of Co and Cr substitution is its oxidation state of trivalent metal, so that it is suggested from these results that the Coulombic interaction between Li/vacancy and the host structure is important in understanding the measurement of dE_{OCP}/dT.

To verify the above assumption, the Monte Carlo simulation that concerns only Coulombic interaction was carried out. The Coulombic term of the lattice enthalpy was expressed by the following equations:

$$U_i = \sum_j \frac{Z_j e}{4\pi\epsilon_0 r_{ij}} \tag{2a}$$

$$U_{\text{Coulomb}} = \sum_{\text{unit cell}} Z_i e U_i \tag{2b}$$

where U_i and U_{Coulomb} indicate the site potential of site i and the total Coulombic energy per unit cell, respectively. Ze is the

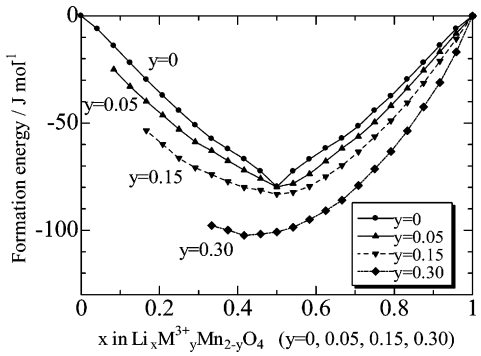

Figure 11. Variation of the formation energy as a function of x in $Li_xM_yMn_{2-y}O_4$.

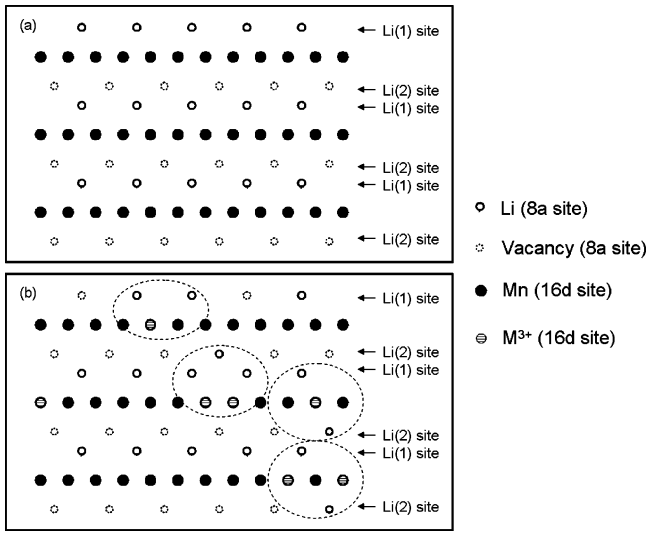

Figure 12. Snapshot of the cation arrangement in (a) $Li_{0.5}Mn_2O_4$ and (b) $Li_{0.5}M_{0.3}Mn_{1.7}O_4$ obtained by Monte Carlo simulation (the figure shows the (110) plane). One can see the perfect ordering of Li/vacancy in 8a tetrahedral sites in panel a, while the break of the ordering was observed in panel b due to the Li cluster formation around M^{3+} cations.

electrical charge of the ions, ϵ_0 is the dielectric constant in a vacuum, and r_{ij} is the interionic distance between ions i and j. In practice, the Ewald method was used for the determination of U_{Coulomb} (this is a method where the conditionally convergent Coulombic sum is transformed into a sum of two rapidly converging sums: a sum in real space and a sum in reciprocal space. Details are described in ref 21). Table 1 shows the structural parameters and oxidation state of modeled crystal $LiM_yMn_{2-y}O_4$. It was assumed that only Mn ions compensate for the electron transfer of redox reaction during charging and discharging, and they possess the averaged oxidation state as listed in Table 1 (the range is +3.5 to +4). The charge Ze of doped metal ions M was fixed as +3, and the random distribution of doped M is assumed as indicated in present XRD results (Figure 2: no peaks arising from superstructure were observed). Note that present simulation method does not consider the repulsive interaction arising from overlapping of electron clouds, van der Waals interaction, and so on, which factors would be included in the formation of the previous approach.[8,10] This makes the present discussion half-quantitative. However, it is worthwhile to point out that the present method enables the simulation without empirical or adjustable parameters, so that one can simulate the electrochemical simulation without experimetal data. In addition, the physical meaning or the origin of the interaction is more apparent, since the present

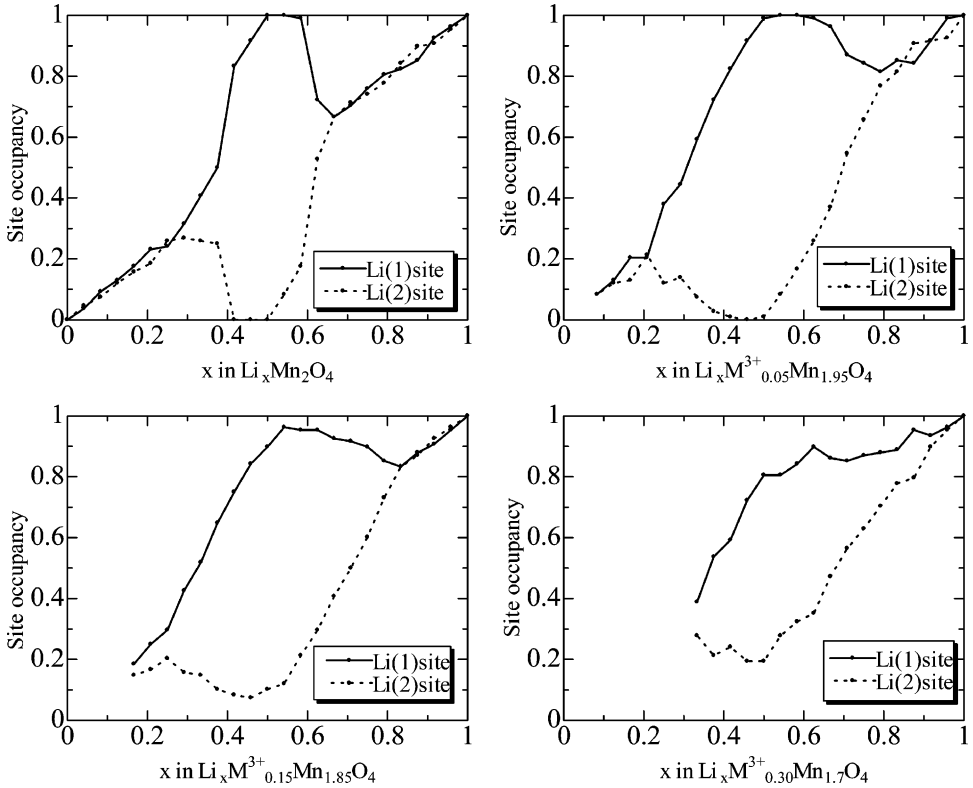

Figure 13. Variation of the site occupancy for Li ions as a function of x in $Li_xM_yMn_{2-y}O_4$. The definitions of Li(1) and Li(2) sites were given in Figure 9.

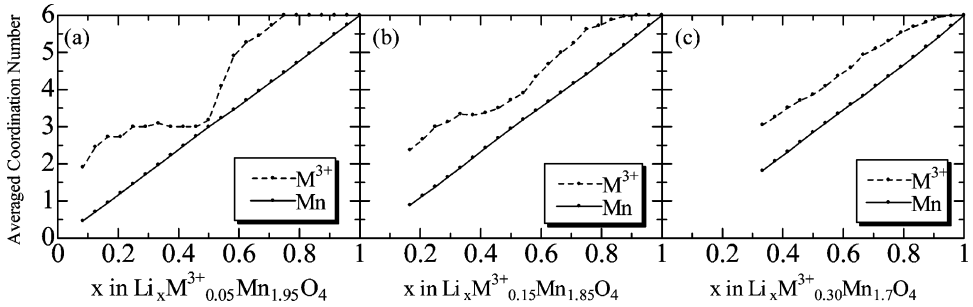

Figure 14. Variation of the averaged coordination number of neighboring Li ions around Mn and M^{3+} cations.

method only considers the Coulombic interaction. By using the Coulombic interaction, the Monte Carlo simulations were performed to determine the appropriate arrangement of Li and vacancy. Nevertheless, it was well-known that the computation of Coulombic interaction takes a long time due to its form of long-range interaction. To reduce the Monte Carlo step, the site u that had relatively larger site-potential U_u was selectively flipped, and only ground-state configuration (i.e., most stable arrangement of Li/vacancy) for each composition x was simulated in this study.

Figure 11 showed the variation of the formation energy in $Li_xM_yMn_{2-y}O_4$, which is defined as obtained Coulombic energy, using Monte Carlo simulation, with subtraction of the Coulombic energy assuming the averaged charge (AVC) distribution listed in Table 1. The results showed convex shaped curves where the energetic minimum was found at $x = 0.5$ for the modeled structure of any composition y. In addition, the resulting formation energy does not vary widely from composition to composition, indicating the present results reproduced the random distribution of Cr statistically. As the composition y increased, the convex function of the formation energy became well-round. Since the derivative of the formation energy corresponds to the OCP, it was expected that the electrochemical reaction proceed via the two voltage region at the border of $x = 0.5$, and substitution of the trivalent metal cation weakens the flat voltage curve at each voltage region observed in $Li_xMn_2O_4$. (In other words, the two-phase coexistence reaction tends to proceed when the number of substituents M^{3+} is small.) Such simulated results qualitatively showed good accordance with the experimental observation as mentioned in the previous section. Accordingly, changes in the voltage as a function of x and y in $Li_xM_yMn_{2-y}O_4$ (M = Co or Cr) around 3.5−4.2 V would be explained solely by the optimization of Coulombic interaction.

To understand the thermodynamic phenomena (Figure 11) from the viewpoint of the atomic level, the arrangement of Li/vacancy at the ground state was investigated. Figure 12a shows a snapshot of Li/Vacancy arrangements in the simulated $Li_{0.5}Mn_2O_4$, showing the ordered arrangement as suggested previously where Li ions alternatingly occupied the tetrahedral 8a site (Figure 9). Figure 13 presents the variation of site occupancy of Li as a function of x in $Li_xMn_2O_4$. Around $x = 1$ and 0, no difference in site occupancy was observed in Li(1) and Li(2) sites, indicating the disordered arrangement of Li/vacancy kept in this region. While the difference increases around intermediate composition x, perfect ordering was indicated in $x = 0.5$ of

Li_xMn_2O, where Li and vacancy sites arrange alternately (Figure 12a). Therefore, the charging reaction of $LiMn_2O_4$ proceeds via three steps: disordering−ordering−disordering of Li/vacancy between Li(1) and Li(2) sites. By adding the substituents of M^{3+}, the difference in site occupation at around $x = 0.5$ was decreased, indicating the M^{3+} ions interrupted the ordered arrangement of Li/vacancies. Such a M^{3+} doping effect would lead to the bending of the potential profile, whereas the perfect ordering of Li/vacancy causes the flat potential at regions I and II in $Li_xMn_2O_4$. To elucidate the effect of trivalent cation M^{3+} for the arrangement of Li/vacancy, the averaged coordination number (averaged CN) of the Li ion, which is the next-neighboring Li of octahedral Mn and M^{3+}, was computed and shown in Figure 14. The linear increase from 0 to 6 in averaged CN of the next neighbor Li is expected as a function of x under the assumption that the distribution of Li ions is independent of that of M^{3+}/Mn ions. The averaged CN of Li around Mn is almost identical with the expectation mentioned above, while that around M^{3+} ions is larger than the expected behavior. On the other hand, the tetrahedral cation sites next to the M^{3+} ions tend to be selectively occupied by the Li ions. Maybe this stems from the smaller repulsive Coulombic interaction between Li and the trivalent M cation than Li and Mn, since the oxidation state of M^{3+} is smaller than that of Mn sites. Hence substituted M^{3+} ions would cause the Li cluster around them, which leads to the break of ordered arrangement of Li/vacancy at composition $x = 0.5$. Figure 12b shows the snapshot of the arrangement of cations in $Li_{0.5}M_yMn_{2-y}O_4$ from the Monte Carlo simulation, and one can see the break of ordered arrangement of Li/vacancy due to the cluster formation of Li around M^{3+} cations. Such a break of Li/vacancy ordering would result in the bending of the potential profile mentioned above. Accordingly, present Monte Carlo simulations revealed that the observed electrochemical behavior of $Li_xM_yMn_{2-y}O_4$ can be understood by the two Coulombic interactions of Li/vacancy ordering and formation of Li cluster around trivalent M ions.

In conclusion, the present study reveals that the macroscopic electrochemical behavior of $Li_xM_yMn_{2-y}O_4$ cathode materials is deeply related to the atomic level Coulombic interactions, which is clarified by the combined experimental and computational techniques. It is worthwhile to stress that Coulombic interaction is one of the key factors in designing materials and predicting the electrochemical behavior from atomic-scale interaction to macroscopic phenomena.

Acknowledgment. The present work was supported in part by the Grant-in-Aid for Scientific Research on Priority Area, Nanoionics (439) by the Ministry of Education, Culture, Sports, and Technology. We would like to thank Mr. Wonkyung Ra and Mr. Harry Locklear for improving the presentation of this paper.

References and Notes

(1) Thackeray, M. M. *Prog. Solid State Chem.* **1997**, *25*, 1
(2) Guyomard, D.; Tarascon, J. M. *Solid State Ionics* **1994**, *69*, 222.
(3) Shimakawa, Y.; Numata, T.; Tabuchi. J. *J. Solid State Chem.* **1997**, *131*, 138.
(4) Abiko, H.; Hibino, M.; Kudo, T. *J. Power Sources* **2002**, *112*, 557.
(5) Masquelier, C.; Tabuchi, M.; Ado, K.; Kanno, R.; Kobayashi, Y.; Maki, Y.; Nakamura, O.; Goodenough, J. B. *J. Solid State Chem.* **1996**, *123*, 255.
(6) Gummow, R. J.; de Kock, A.; Thackeray, M. M. *Solid State Ionics* **1994**, *69*, 59.
(7) Ohzuku, T.; Kitagawa, M.; Hirai, T. *J. Electrochem. Soc.* **1990**, *137*, 3769.
(8) Gao, Y.; Reimers, J. N.; Dahn, J. R. *Phys. Rev. B* **1996**, *54*, 3878.
(9) Thomas, K. E.; Bogatu, C.; Newman, J. *J. Electrochem. Soc.* **2001**, *148*, A570.
(10) Wong, W. C.; Newman, J. *J. E.ectrochem. Soc.* **2002**, *149*, A493.
(11) Van der Ven, A.; Ceder, G. *Solid State Ionics* **2000**, *135*, 21.
(12) Ammundsen, B.; Burns, G. R.; Islam, M. S.; Kanoh, H.; Rozière, J. *J. Phys. Chem. B* **1999**, *103*, 5175.
(13) Liu, W.; Kowal, K.; Farrington, G. C. *J. Electrochem. Soc.* **1998**, *145*, 459.
(14) Berg, H.; Thomas, J. O. *Solid State Ionics* **1999**, *126*, 227.
(15) Guohua, L.; Ikuta, H.; Uchida, T.; Wakihara, M. *J. Electrochem. Soc.* **1996**, *143*, 178.
(16) Kaneko, M.; Matsuno, S.; Miki, T.; Nakayama, M.; Ikuta, H.; Uchimoto, Y.; Wakihara, M.; Kawamura, K. *J. Phys. Chem. B* **2003**, *107*, 1727.
(17) Nakayama, M.; Kaneko, M.; Uchimoto, Y.; Wakihara, M.; Kawamura, K. *J. Phys. Chem. B* **2004**, *108*, 3754.
(18) Wang, Z.; Ikuta, H.; Uchimoto, Y.; Wakihara, M. *J. Electrochem. Soc.* **2003**, *150*, A1250.
(19) Su, Y. C.; Zou, Q. F.; Wang, Y. W.; Yu, P.; Liu, J. Y. *Mater. Chem. Phys.* **2004**, *84*, 302.
(20) Shannon, R. D. *Acta Crystallogr.* **1976**, *A32*, 751.
(21) Kittel, C. *Introduction to Solid State Physics*; Wiley: New York, 1996.